ADVANCED ELECTRONIC MATERIALS
Open Access
www.advelectronicmat.de

Thermometry of AlGaN/GaN 2D Channels at High Electric Fields Using Electrical and Optical Methods

S. Vitusevich, I.M. Nasieka, A. V. Naumov, V. V. Kalyuzhnyi, O. I. Liubchenko, I. O. Antypov, M. I. Boyko, and A. E. Belyaev*

The active channels in AlGaN/GaN-based heterostructures are studied under different applied electrical fields to identify the Joule heating factors affecting the temperature values in the channels. The temperature in active channels of two different lengths (30 and 180 µm) is characterized using optical methods, and electrical methods are used as a reference. The technique of optical thermometry is based on the data of micro-photoluminescence and micro-Raman experiments. The electrical method is based on the measurements of current–voltage characteristics for comparison. It is shown that photoluminescence- and electrical-based temperature values demonstrate similar behavior and good correlation. The Raman-based method, exploiting the temperature dependence of the frequency position of E_2^{high} vibrational band in GaN, shows a significant deviation compared with electrical- and luminescence-based methods. This deviation is shown to be related to the residual mechanical strain in the layered structure and the formation of hot phonons. The influence of hot phonons and mechanical strain effects increases at high electrical load (>5 kV cm^{-1}) and at high temperatures (>400 °C), respectively.

1. Introduction

Determining the temperature in the components of optoelectronic devices at an applied voltage within the range corresponding to the predicted operational modes is an important task because the temperature is one of the main factors that negatively affect device performance and often leads to its degradation. The challenge of temperature control is highly relevant in high electron mobility transistors (HEMT) based on AlGaN/GaN heterostructures, particularly in HEMT-based biosensors.[1–5] The response of HEMT-based biosensors is strongly dependent on the device temperature and applied electrical field.[5] The essential peculiarity of such devices is the formation of 2D electron gas (2DEG) at the AlGaN/GaN interface. The conducting channel with 2DEG operating at high electrical fields heats up due to the Joule effect. In this case, temperature gradients as high as 100 °C µm^{-1} can be present close to the device channel, which can change the biosensor performance enough to cause an error in sensor response. This can be manifested, for example, in the incorrect determination of a certain analyte density.[5] The second effect that causes a temperature increase in the conduction channel is the formation of hot electrons and hot phonons, which decreases the efficiency of heat dissipation and reduces the electron saturation velocity.[6–16] In AlGaN/GaN conduction channels, the following physical mechanisms also cause performance degradation: electrical, mechanical, and environmental. However, thermal-induced degradation is dominating.[2] Therefore, controlling the temperature in the AlGaN/GaN channels is an essential task for obtaining the maximum operating temperature and predicting the device's lifetime to optimize operating conditions, particularly in HEMT-based biosensors.

Four experimental methods allow temperature estimation in electronic devices: infrared (IR) thermometry (the most commonly used), micro-photoluminescence (µ-PL) method, an electrical method based on measurements of the current–voltage characteristics (CVCs), and micro-Raman (µ-RS) thermometry.[2,3,17] Surely, all of these techniques have both advantages and disadvantages. In IR-thermometry, the spatial resolution is in the order of the wavelength measured (3–10 µm). It reflects

S. Vitusevich
Institute of Biological Information Processing (Bioelectronics (IBI-3)
Forschungszentrum Juelich D
52425 Juelich, Germany
E-mail: s.vitusevich@fz-juelich.de

I.M. Nasieka, V. V. Kalyuzhnyi, O. I. Liubchenko,
M. I. Boyko, A. E. Belyaev
V.Ye. Lashkaryov Institute of Semiconductor Physics of NAS of Ukraine
41 Nauki Ave, 03028 Kyiv, Ukraine

I.M. Nasieka, I. O. Antypov
National University of Life and Environmental Sciences of Ukraine
Education and Research Institute of Energetics
Automation and Energy Efficiency
12 Heroyiv Oborony str., 03041 Kyiv, Ukraine

A. V. Naumov
AGH University of Science and Technology
Academic Centre for Materials and Nanotechnology
al. Mickiewicza 30, 30-059 Krakow, Poland

The ORCID identification number(s) for the author(s) of this article can be found under https://doi.org/10.1002/aelm.202201330.

DOI: 10.1002/aelm.202201330

a limitation in the temperature interpretation at long wavelengths for testing the devices with submicron components.[3] In IR thermometry, the lateral and depth temperatures are averaged, resulting in lower values of measured data points compared to the actual peak temperature.[2,3] The μ-PL thermometry is based on an analysis of the temperature dependence of the band-edge emission, excited by the laser with a wavelength above the energy band gap (E_g). The use of a confocal microscope can reduce the diameter of the excitation spot to 1.5 μm, providing a spatial resolution close to 1 μm or less. This technique is better than IR thermometry, but exploiting the laser with a wavelength above the corresponding E_g leads to current/field redistribution in the channel where the temperature is being measured due to the generation of additional electron–hole pairs. The photo-induced current causes heating of the device in addition to direct laser heating of the sample surface.[3,17] The above-listed methods provide the averaged integral temperature of the device. In contrast, μ-RS thermometry is deemed the most accurate method for temperature estimation in the working channels of AlGaN/GaN heterostructures.[2–5] The main advantage of the μ-RS method compared to the μ-PL method is the possibility of using the below-band-gap excitation, avoiding intensive light absorption and additional laser-induced heating.[17] Although methods of heat removal from the 2D channels have already been proposed, the active factors influencing the temperature, obtained using the most accurate μ-RS method, have not been studied sufficiently.[18–20]

In this paper, we present an analysis of different factors in the μ-RS thermometry experiments, including residual thermal strain, which affects the accuracy of temperature measurements. The electrical method is used as the reference technique.[2,21–24]It is demonstrated that the mechanical strain, which can reach 50 MPa (and can induce the shift equal to 21.1 meV GPa^{-1}) in the AlGaN/GaN heterostructure influences the frequency of Raman modes, PL peak position, and the formation of the "hot spots." In addition, the Raman testing depth and hot electrons are taken into account.

2. Experimental Section

The studied AlGaN/GaN heterostructures were grown on the 450 μm thick Al_2O_3 single crystalline substrate using the metal-organic chemical vapor deposition (MOCVD). **Figure 1**a shows the schematic presentation of the structure of the studied samples and the density of the electronic states in their energy band. The heterostructure consists of a single crystalline undoped GaN buffer layer (3 μm), $Al_{0.3}Ga_{0.7}N$ barrier layer (30 nm), and GaN undoped cap layer (4 nm). It was important for us to show the formation of 2D electron gas (2DEG) with excellent electrical parameters. For this reason, we present the sequence of the layers with the nominal thicknesses in the text. Nevertheless, we examined the heterostructure using high-resolution transmission electron microscopy (HRTEM) as well as X-Ray diffraction (not presented in the text). Measured and nominal thicknesses correlate well within 1–2 monolayers.

The conducting channels of different lengths (30 and 180 μm) and the Hall-bar pattern for 2DEG characterization, formed using photolithography on the surface of the AlGaN/GaN heterostructure, are shown in Figure 1b. The theoretical calculations of the energy band structure show that 2DEG is localized within a 2–4 nm layer in an asymmetrical quantum well at the GaN/AlGaN interface[25] and penetration of the wave function of 2DEG into the barrier is negligible. Thus, the effect of the interface roughness can be neglected.

The transport properties of 2DEG were obtained using Hall measurements: electron mobility $\mu_{300\ K} = 1260\ cm^2\ V^{-1}\ s^{-1}$, concentration $n_S = 1.02 \times 10^{13}\ cm^{-2}$.

For μ-PL measurements, the 325 nm (≈3.8 eV is approximately equal to the $E_g(Al_{0.3}Ga_{0.7}N)$) line of the He–Cd laser was used with the relatively small laser power density of ≈50 μW μm^{-2} as an excitation tool. To prevent laser heating, the μ-RS measurements were performed under 488 nm (2.54 eV) excitation of the Ar–Kr laser.[26–30] In these conditions, the vertical absorption depth in the GaN is ≈80 nm.[17] The spectrometer HORIBA Jobin-Yvon T64000 equipped with a confocal microscope and

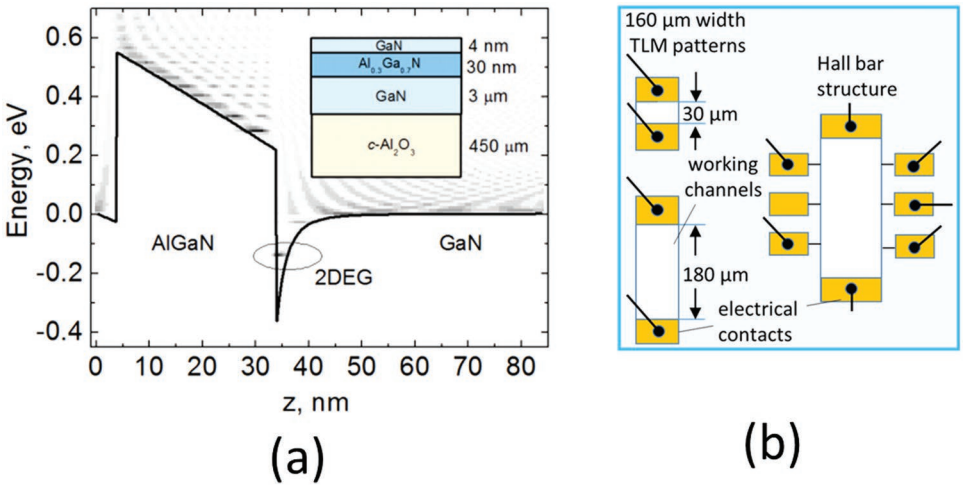

Figure 1. a) Schematic presentation of the layout structure of the studied samples, potential profile of the structure, and corresponding electronic state density; b) schematic view of the working channels on the sample surface. Yellow areas are the electrical contacts formed by photolithography in the following order: Ti(35 nm)/Al (200 nm)/Ni (45 nm)/Au (100 nm); AlGaN/GaN channels are shown in white.

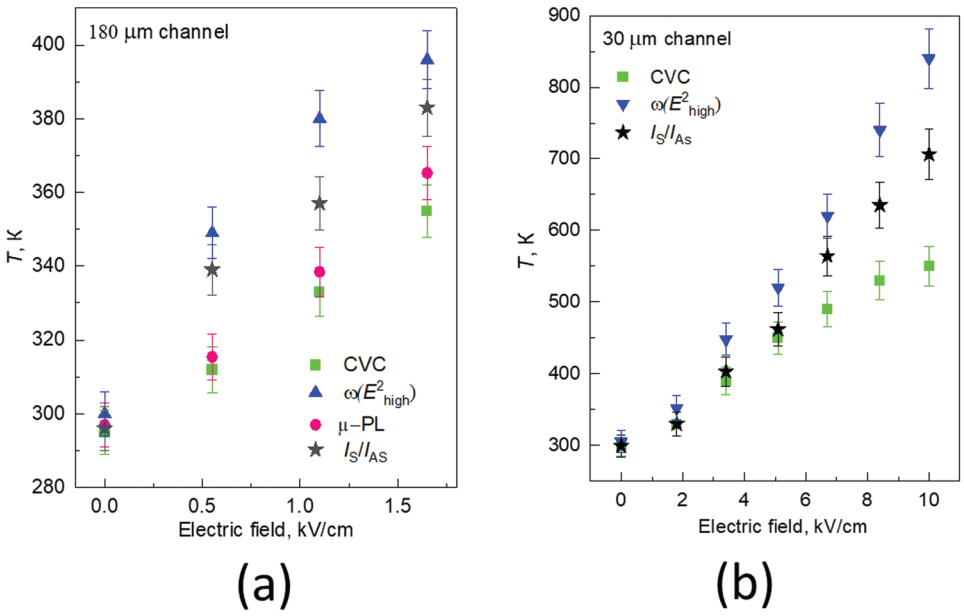

Figure 2. The temperature in AlGaN/GaN channels as a function of the electric field, obtained using the electrical method (green points) and the optical method for different channel lengths: a) 180 μm length and b) 30 μm length. The optically obtained temperature data (black, blue, and red points) will be discussed below.

Peltier cooled ANDOR CCD camera was used for spectra registration and laser beam focusing. To tune the temperature, the Linkam THM600 thermostat equipped with a thermal contact plate for heat transfer was used. The μ-PL and μ-RS spectra were measured in backscattering geometry.

3. Results and Discussion

3.1. Electrical Evaluation of the Temperature

The electrical method was chosen as the reference method for temperature evaluation because the electrical properties of the structure determine the device performance edges. The electrical method is based on the calculation of thermal conductivity, considering thermal diffusion and dissipation.[22,31] It is well known that the dissipated power as the result of heat dissipation during the flow of current can be expressed as $P_{\text{dis}} = I \cdot E \cdot L$, where L is the length of the conductive channel, I is the current in the channel, and $E = \frac{U}{L}$ is the average electric strength in the channel. The temperature increase per 1 Watt is equal to $\Theta = \frac{\Delta T}{P_{dis}}$, where $\Delta T = T - T_0$, T is the temperature of the active region heated by 2DEG, and T_0 is the temperature of the effective thermal contact.

Figure 2 shows the temperature of active regions as a function of the applied electric field for conducting channels of different lengths. The data was obtained by analyzing the CVCs and optical measurements. One can see that for both channels, there is a monotonic increase in temperature with an increase in the applied electric field. The experimental temperature data points are located within the same temperature range reported by Kuball in ref. [3], Pavlidis in ref. [4], and Cutivet in ref. [6] despite the authors using a different electrical method—gate resistance measurement (GRM). An insubstantial mismatch between our temperature data and those reported in refs. [3–5] can be explained by the difference in the shape and the size of active channels.

3.2. Optical Methods for Temperature Determination

3.2.1. Photoluminescence-Based Thermometry

Optical temperature determination is based on the techniques of μ-RS and μ-PL. We used the method of μ-PL, intending to compare its results with the μ-RS method. The μ-PL method is based on the temperature dependence of the band-edge PL peak (donor-bound exciton emission D^0X) position in the spectra of the studied AlGaN/GaN heterostructure (calibration curve). The calibration process includes measurements of the μ-PL spectra of the AlGaN/GaN with no electrical load in the thermostat with the temperature-controlled unit in the chamber. The calibration curve allows the evaluation of temperature using the position of the band-edge PL peak measured at the electrical load.

Figure 3a shows the calibration curve (aquamarine dots with black borders) and the curve plotted according to the modified Varshni equation (red solid line)[1,2,17]

$$E = E_0 - \frac{\alpha T^2}{T + \beta} + \frac{1}{2}kT \quad (1)$$

where E is the D^0X peak position at temperature T, k is the Boltzmann constant, and α, E_0, and β are empirical fitting parameters. The term $\frac{1}{2}kTs$ describes the kinetic energy of the carriers when they recombine in the GaN layer. In our case, the fitting parameters are as follows: $\alpha = 7.5 \cdot 10^{-4}$, $E_0 = 3.475$ eV, and $\beta = 1000$.

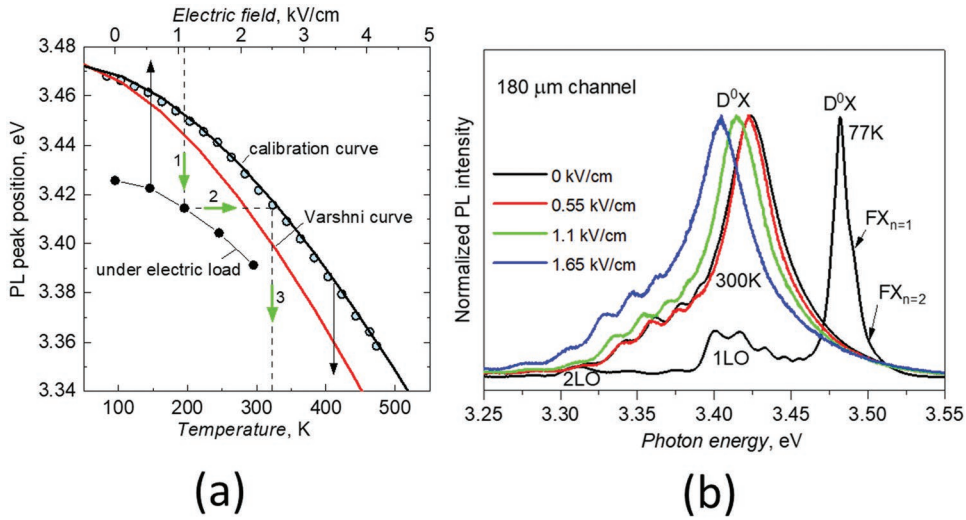

Figure 3. a) The temperature dependencies of the D^0X peak position: calibration curve (aquamarine dots), Varshni curve (red solid line), and the curve obtained under the electric load (black filled dots). b) Liquid nitrogen and room-temperature μ-PL spectra of AlGaN/GaN/Al_2O_3 structure were measured at different applied electric fields (color curves) and with no electric field (black curve).

It should be noted that in obtaining the calibration curve, we consider the influence of the mechanical strain in the heterostructure AlGaN/GaN on the energy band gap (E_g). This influence is manifested as the declination of the calibration curve (with strain consideration) from the standard Varshni curve (in the absence of strain; see Figure 3a). The noted declination is caused by the specific strain-induced spectral shift, which can reach a value of up to 21.1 meV GPa^{-1}.[17] The black dots designate the PL peak positions measured at the applied electric load. Green arrows show the logical scheme for determining the temperature in the 2DEG channel using the three following steps. Step 1 involves the determination of the PL peak position under the particular electric field. Then, we move horizontally to the intersection with the calibration curve (step 2), and finally, go vertically down to the intersection with the temperature axis (step 3).

Figure 3b demonstrates the normalized μ-PL spectra of the studied AlGaN/GaN/Al_2O_3 structure measured at 77 K and 300 K at the applied electrical field within the range up to 1.65 kV cm^{-1} and with no electrical field. The sample had a channel length of 180 μm (an excitation spot diameter was less than 2 μm). The low-temperature spectrum consists of the dominating donor-bound exciton emission band with a peak centered at 3.48 eV.[28,29] The asymmetry from the right side is caused by the emission attributed to the annihilation of free excitons $FX_{n\ =\ 1,2}$. The corresponding bands are positioned approximately at 3.49 eV and 3.51 eV, respectively. The multipeak bands within the range 3.4–3.45 and 3.3–3.35 eV are probably caused by the superposition of the LO-phonon replicas of the exciton-related bands.[27–31] LO phonon energy is about 90 meV.

To prevent the liquid nitrogen-induced cooling of the samples heated by the electric current, all μ-PL measurements under the applied electric field were performed at room temperature. At room temperature, μ-PL spectrum of the GaN-based structure dominates with a single donor-bound exciton (D^0X) emission band at 3.42 eV.[27–31] Applying the electric field leads to the peak red shift of the D^0X band within the range 3.42–3.40 eV at electric fields up to 1.65 kV cm^{-1}. The mentioned shift is caused by the temperature increase due to Joule self-heating and the mechanical strain increase in the AlGaN/GaN heterostructure.[32–34] The temperature data points obtained using the μ-PL method are plotted in Figure 2a as red dots. CVC and μ-PL points show a good correlation, proving the idea that the calibration curve considers the increasing strain influence. It should be noted that to minimize the direct laser heating of the sample, we exploited a relatively small laser power density of ≈50 μW $μm^{-2}$.[14] In ref. [13], the authors reported a very small laser-induced temperature rise (up to 5 °C) in AlGaN/GaN-based devices at the excitation laser densities equal to 0.14 μW $μm^{-2}$. The temperature caused by laser heating monotonically increases with increasing bias voltage. Thus, we can conclude that the deviation between temperature data points obtained using the CVC and μ-PL methods observed in Figure 2a can be explained by the laser heating effect.

3.2.2. Raman Scattering-Based Thermometry

Figure 4 presents the room-temperature Stokes and anti-Stokes μ-RS spectrum of AlGaN/GaN heterostructure measured in the 180 μm active channel with no electrical load. The Stokes lines are always significantly higher in intensity than their anti-Stokes counterparts.[35]

Therefore, we multiplied the intensity of the anti-Stokes line by 10 for demonstration. Instead of typical GaN-associated vibrational bands A_1^{LO}, E_2^{low}, and E_2^{high}, the vibrational band at 514.2 cm^{-1} in the Stokes region was registered. This is a manifestation of the sapphire substrate and was attributed to the E_g mode.[36,37] The active channel temperature can be found as the ratio $\frac{I_S}{I_{a-S}}$ of the intensities (Stokes and anti-Stokes) of the vibrational bands in the corresponding Raman spectra due to the strong dependence of the anti-Stokes intensity on the ambient temperature following the equation

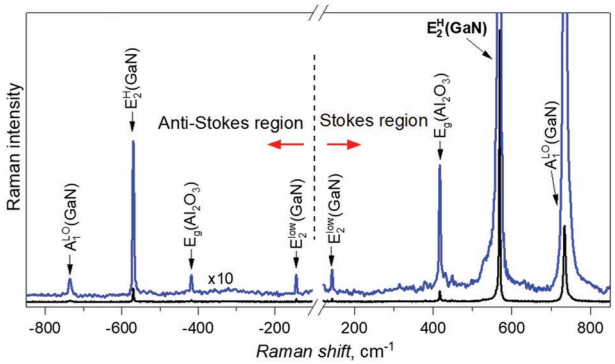

Figure 4. Room-temperature Stokes and anti-Stokes μ-RS spectra measured for 180 μm active channel with no electrical load.

$$\frac{I_S}{I_{a-S}} = C\left(\frac{\omega_l + \omega_S(T)}{\omega_l - \omega_S(T)}\right)^4 \cdot \exp\left(\frac{\hbar\omega_S(T)}{kT}\right) \quad (2)$$

where ω_l, ω_S are the frequencies of the exciting laser emission and the Stokes component of the vibrational band E_2^{high}, respectively.[38,39] The constant C (strength of phonon oscillator) is determined by the experimental conditions such as the efficiency of light scattering, the spectral sensitivity of the spectrometer, etc. Equation (2) allows estimating the phonon temperature in the case of the presence of the hot phonons.[7–16] The phonon temperature is equal to the lattice temperature without hot phonons. In the case of the presence of nonequilibrium hot phonons, the obtained temperature will be higher than the lattice temperature. The temperature data points obtained using Equation (2) are shown in Figure 2a,b using black asterisks. The temperature obtained using $\frac{I_S}{I_{a-S}}$ is slightly higher than using μ-PL and CVCs data. Considering the results of a comprehensive investigation of AlGaN/GaN heterostructures presented by Kosemura in ref. [40] and Tripathy in refs. [21] and [41], the presence of the mechanical strain affects only the shift and splitting of phonon modes. At the same time, the Raman intensities remain unchanged. Consequently, the difference in the temperature data points obtained using CVC and μ-PL methods, on the one hand, and obtained using the ratio $\frac{I_S}{I_{a-S}}$, on the other, can be explained by the generation of hot electrons and hot phonons. It should be noted that the value of the obtained temperature deviation increases with increasing electric field strength.

Another method for temperature determination using the experimental μ-RS spectra is the analysis of the temperature dependence of the peak position of the E_2^{high} vibrational band, which can be described using the semi-empirical equation reported in refs. [3], [20], and [40]

$$\omega(T) = \omega_0 - \frac{A}{\exp\left(\frac{B\hbar c\omega_0}{kT}\right) - 1} \quad (3)$$

where ω_0 is the frequency of E_2^{high} vibrational band at $T = 0$ K and k is the Boltzmann constant. A and B are empirical fitting parameters and in our case $A = 0.01\ cm^{-1}$, $B = 0.19\ cm^{-1}$. Using Equation (3), we can find the temperature in the active channel of a sample

$$T = \frac{B\hbar c\omega_0}{k\ln\left(1 + \frac{A}{\omega_0 - \omega(T)}\right)} \quad (4)$$

Equation (4) has the same functional form as the temperature dependence of the energy band gap taking into account only electron–phonon interaction (Einstein simplification) and does not consider the influence of mechanical strain.[42] The temperature data points according to Equation (4) are shown in Figure 2a,b as blue triangles. The deviation between points obtained using CVCs, μ-PL, and E_2^{high} frequency can be explained as follows.

Firstly, for the selection of parameters A and B, the data for samples heated in the thermostat with no electrical load are used. In the thermostat, the temperature sensor was placed on the thermally conductive plate. The samples were placed on the surface of the plate. When estimating parameters A and B, some errors should be taken into account due to the temperature gradient during sample heating. The contact of the samples with air also influences the measurements because the thermostat is not evacuated. Secondly, direct laser heating occurs, which can influence the values of A and B. However, these two factors are technical and can be proved experimentally. Both factors cause unsubstantial (up to 5 K) deviation in the temperature.

In addition to these two factors, there is an important physical factor that has to be be considered: the influence of internal mechanical strain on the frequency position of the E_2^{high} vibrational band. The studied AlGaN/GaN heterostructures are multilayered and have an internal mechanical strain, which includes two components. The first component is determined by the lattice mismatch between the hetero-layers and substrate, and the second is due to the difference in the coefficient of thermal expansion of the GaN-based material and sapphire substrate.[2,40] Both factors induce the total mechanical strain, which should be estimated during temperature evaluation using the μ-RS method.

Hence, the strain-induced shift of the frequency position of the E_2^{high} band $\Delta\omega_{str}$ includes two components: $\Delta\omega_{miss}$ which is attributed to the lattice mismatch and $\Delta\omega_{expan}$ which is attributed to the difference in the thermal expansion coefficients. The dependence of frequency position E_2^{high} band can be described as

$$\omega(T) = \omega_0 - \Delta\omega_d(T) - \Delta\omega_{str}(T) \quad (5)$$

where $\Delta\omega_{str} = \Delta\omega_{mis} + \Delta\omega_{expan}$ and $\Delta\omega_d$ is the frequency shift due to the electron–phonon interaction and phonon delay processes, which can be expressed using Equation (3) as $\Delta\omega_d = \frac{A}{\exp(\frac{B\hbar c\omega_0}{kT}) - 1}$.[2,40] To describe the frequency shift component due to the total internal strain, the well-known relation can be used

$$\Delta\omega_{str}(T) = 2\left(a - b\frac{C_{13}}{C_{33}}\right)\cdot\varepsilon(T) \quad (6)$$

where a and b are the phonon deformation potentials, C_{13} and C_{33} are the elastic constants of the studied layer, and $\varepsilon(T)$ is the strain. The phonon deformation potentials for the E_2^{high} band were previously determined in ref. [43] (see Table II). They have the following values: $a = -1027\ cm^{-1}$, $b = -597\ cm^{-1}$.

ADVANCED ELECTRONIC MATERIALS
Open Access
www.advelectronicmat.de

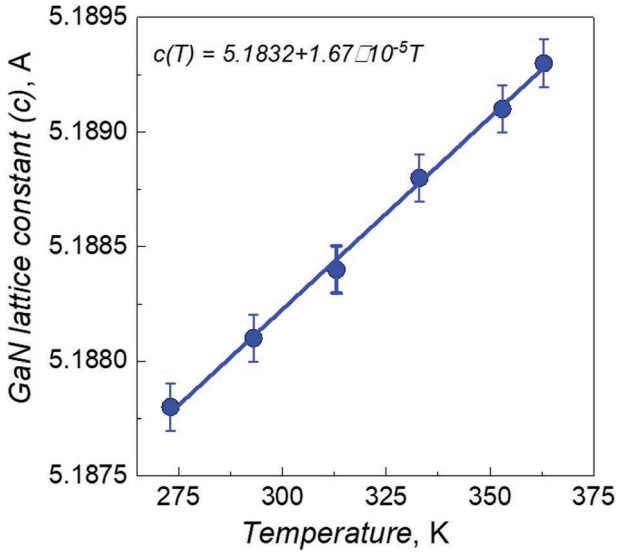

Figure 5. The temperature dependencies of the lattice parameter of GaN in the heterostructure AlGaN/GaN/Al_2O_3.

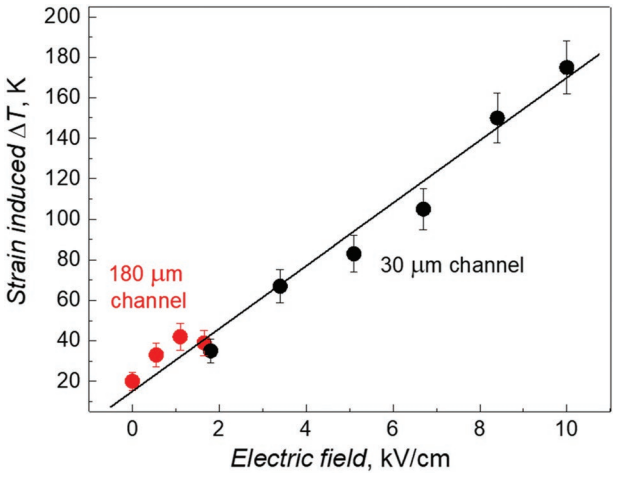

Figure 6. Strain-induced temperature correction as a function of the electric field, calculated using Equation (8) for samples with different channel lengths: 180 μm (red dots) and 30 μm (black dots).

For the similar GaN layer, the elastic constants are: $C_{13} = 106$, $C_{33} = 398$. Using the values of the above-listed constants, we can summarize that $\Delta\omega_{str}(T) = -1736 \cdot \varepsilon(T)$. We should then find the corresponding value of the internal strain.

The strain in the studied heterostructure can be evaluated using the expression $\varepsilon(T) = \frac{c(T) - c_0}{c_0}$, which describes the relative elongation of the lattice parameter c in the GaN layer measured using X-ray diffractometry. In this case, c_0 is the lattice parameter according to 0002 GaN reflex at $T = 0$ K and c is the GaN lattice parameter measured at a certain temperature.

Figure 5 shows the GaN lattice parameter c as a function of temperature for the studied AlGaN/GaN heterostructure. The dependence c demonstrates linear behavior, which can be described by the expression $c(T) = 5.1832 + 1.67 \cdot 10^{-5} T$. This reflects that $c_0 = 5.1832$ Å and the frequency shift due to mechanical strain can be expressed as $\Delta\omega_{str}(T) = -0.005 \cdot T$. Using the latter, Equation (3) for the temperature evaluation can be written as

$$T = \frac{B\hbar c\omega_0}{k \ln\left(1 + \frac{A}{\omega_0 - \omega(T) - 0.005 \cdot T}\right)} \quad (7)$$

The term $0.005 \cdot T$ is the function of temperature. The next question to be answered is therefore the temperature that should be considered. In this case, the temperature data points obtained using the CVC experiments should be used. For a clear demonstration of the influence of the strain on the evaluated temperature, the difference in the temperature values (ΔT_{str}) obtained using the frequency position of the E_2^{high} band in strained and unstrained cases is

$$\Delta T_{str} = \frac{B\hbar c\omega_0}{k}\left(\frac{1}{\ln\left(1 + \frac{A}{\omega_0 - \omega(T)}\right)} - \frac{1}{\ln\left(1 + \frac{A}{\omega_0 - \omega(T) - 0.005 \cdot T}\right)}\right) \quad (8)$$

Figure 6 presents, the calculated data of electric-field dependence of the temperature correction ΔT_{str} due to mechanical strain, which increases with an increasing electrical field, obtained for both samples with 180 μm and 30 μm active channels.

To demonstrate the relation between the temperature data points obtained using the CVCs and Raman experiments with strain and no strain, we summarize the data in **Figure 7**. In the 180 μm active channel, the data points obtained using the frequency position of the E_2^{high} band after the temperature correction are similar to the data points obtained using CVCs under the electrical field, increasing up to 1.65 kV cm^{-1}.

In the 30 μm channel, the temperature measurements were performed in an expanded range of electrical field (up to 10 kV cm^{-1}). Within the range of up to 7 kV cm^{-1}, the proposed temperature correction allows us to adjust the data points obtained using the frequency position of the noted Raman band to the points obtained using the electrical method. Within the range of 7–10 kV cm^{-1}, there is a substantial mismatch between optically and electrically obtained temperature values. Moreover, this mismatch increases with increasing electrical load. The maximum mismatch is observed at 10 kV cm^{-1} and is 115 °C. This effect can be explained by the increasing role of hot phonons, which cause an increase in the average phonon temperature.[7–16] When hot phonons are generated, the phonon temperature already differs from the lattice temperature. This mismatch increases with an increasing concentration of hot phonons. In ref. [22], it is demonstrated that how the influence of hot electrons, hot phonons, and the self-heating effect can be separated. It was shown that the impact of hot electrons in the temperature mismatch can be similar to the impact of the strain at high electrical fields. In our case, at the highest electrical field (10 kV cm^{-1}), the contribution of hot phonons to the mismatch between the temperature data points is about 40%.

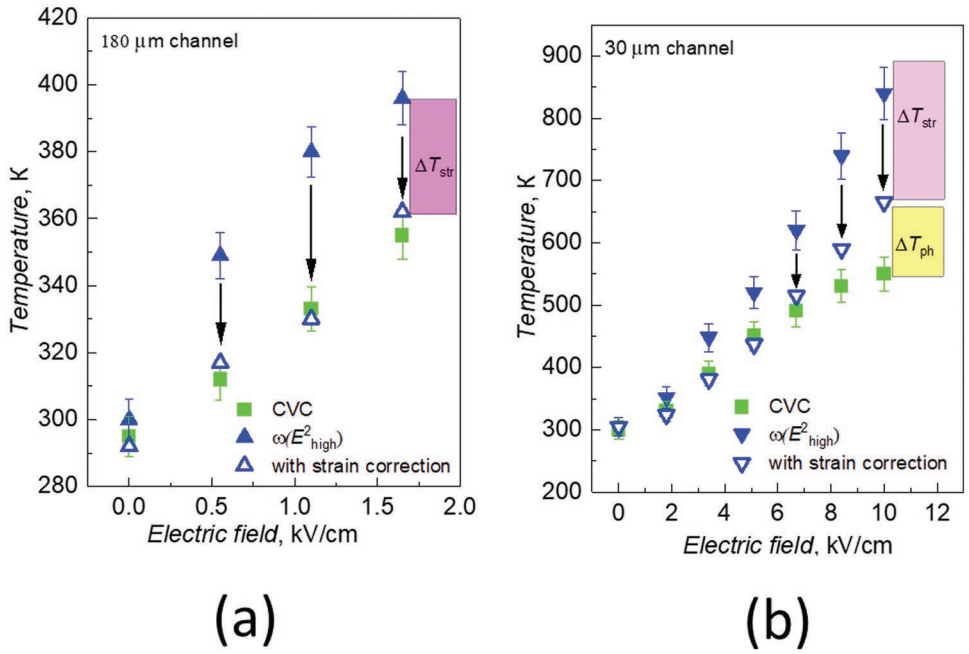

Figure 7. The temperature data points obtained using CVCs (green points) as well as the frequency position of the E^2_{high} band with internal strain (unfilled triangles with blue borders) and with no strain (filled blue triangles) for different channel lengths: a) 180 μm and b) 30 μm.

4. Conclusions

The temperature rise in the active channels of AlGaN/GaN gateless heterostructures caused by the electrical fields in the range up to 10 kV cm^{-1} was investigated using several experimental methods: current–voltage characteristics, noncontact optical micro-photoluminescence, and micro-Raman scattering methods. The obtained temperature data points in the CVC and μ-PL methods were in good agreement. In contrast, μ-RS results demonstrated a significant deviation compared to data obtained using the CVC and μ-PL methods. This temperature mismatch (40–300 °C depending on the active channel length and the applied electric field) was defined as the influence of the residual internal strain and hot phonons, the contributions of which can be estimated according to the ratio of 3:2 at the highest electrical field of 10 kV cm^{-1} in the present study. These results should be taken into account for understanding the specificity of the temperature determination in the HEMTs and HEMT-based biosensors, fabricated on the III-nitrides, particularly in multilayered structures with complex uncompensated residual strain, using the Raman scattering method.

Acknowledgements

Open access funding enabled and organized by Projekt DEAL.

Conflict of Interest

The authors declare no conflict of interest.

Data Availability Statement

The data that support the findings of this study are available from the corresponding author upon reasonable request.

Keywords

AlGaN/GaN heterostructures, Joule self-heating, micro-photoluminescence, micro-Raman scattering, thermometry

Received: December 16, 2022
Revised: March 3, 2023
Published online: April 19, 2023

[1] N. Shigekawa, K. Onodera, K. Shiojima, *Jpn. J. Appl. Phys.* **2003**, *42*, 2245.
[2] T. E. Beechem, *Ph.D. Thesis*, Georgia Institute of Technology **2008**.
[3] M. Kuball, J. Pomeroy, *IEEE Trans. Device Mater. Reliab.* **2016**, *16*, 667.
[4] G. Pavlidis, S. Pavlidis, E. Heller, E. Moore, R. Vetury, S. Graham, *IEEE Trans. Electron Devices* **2017**, *64*, 78.
[5] K. Upadhyay, M. Chattopadhyay, *Mater. Sci. Eng. B* **2021**, *263*, 114849.
[6] Cutivet, F. C. , M. Bouchilaoun, A. Chakroun, O. Arenas, M. Lesecq, J.-C. de Jaeger, A. Jaouad, F. Boone, H. Maher, *IEEE Electron Device Lett.* **2017**, *38*, 240.
[7] A. Matulionis, J. Liberis, I. Matulioniene, M. Ramonas, L. Eastman, J. Shealy, V. Tilak, A. Vertiatchikh, *Phys. Rev. B* **2003**, *68*, 035338.
[8] M. Ramonas, A. Matulionis, L. Rota, *Semicond. Sci. Technol.* **2003**, *18*, 118.
[9] V. Aninkevicius, A. Matulionis, I. Matulioniene, *Semicond. Sci. Technol.* **2005**, *20*, 109.

[10] M. Ramonas, A. Matulionis, J. Liberis, L. Eastman, X. Chen, Y. Sun, *Phys. Rev. B* **2005**, *71*, 075324.
[11] A. Matulionis, *Phys. Status Solidi A* **2006**, *203*, 2313.
[12] K. Wang, J. Simon, N. Goel, D. Jena, *Appl. Phys. Lett.* **2006**, *88*, 022103.
[13] A. Matulionis, H. Morkoc, *Proc. SPIE* **2009**, *7216*, 721608.
[14] G. Xu, S. Tripathy, X. Mu, Y. Ding, K. Wang, Yu. Cao, D. Jena, J. Khurgin, *Laser Phys.* **2009**, *19*, 745.
[15] E. Sermuksnis, J. Liberis, A. Matulionis, V. Avrutin, R. Ferreyra, U. Ozgur, H. Morkoc, *Semicond. Sci. Technol.* **2015**, *30*, 035003.
[16] A. Dyson, D. Naylor, B. Ridley, *IEEE Trans. Electron Devices* **2015**, *62*, 3613.
[17] T. Batten, A. Manoi, M. Uren, T. Martin, M. Kubal, *J. Appl. Phys.* **2010**, *107*, 074502.
[18] L. Arivazhagan, A. Jarndal, D. Nirmal, *J Comput Electron* **2021**, *20*, 873.
[19] L. Sang, *Funct. Diamond* **2021**, *1*, 174.
[20] J. Yaita, A. Yamada, J. Kotani, *Jpn. J. Appl. Phys.* **2021**, *60*, 076502.
[21] S. Tripathy, S. Chua, P. Chen, Z. Miao, *J. Appl. Phys.* **2002**, *92*, 3503.
[22] S. Vitusevich, S. Danylyuk, N. Klein, M. Petrychuk, A. Avksentyev, V. Sokolov, V. Kochelap, A. Belyaev, V. Tilak, J. Smart, A. Vertiatchikh, L. Eastman, *Appl. Phys. Lett.* **2003**, *82*, 748.
[23] T. Beechem, A. Christensen, S. Graham, D. Green, *J. Appl. Phys.* **2008**, *103*, 124501.
[24] T. Beechem, A. Christensen, D. Green, S. Graham, *J. Appl. Phys.* **2009**, *106*, 114509.
[25] A. Naumov, O. Kolomys, A. Romanyuk, B. Tsykaniuk, V. Strelchuk, M. Trius, A. Avksentyev, A. Belyaev, *Semicond. Phys. Quantum Electron. Optoelectron.* **2015**, *18*, 396.
[26] A. Zubrilov, Yu. Melnik, A. Nikolaev, M. Jacobson, D. Nelson, V. Dmitriev, *Semiconductors* **1999**, *33*, 1067.
[27] M. Reshchikov, H. Morkoc, *J. Appl. Phys.* **2005**, *97*, 061301.
[28] L. Tung, K. Lin, E. Chang, W. Huang, Y. Hsiao, C. Chiang, *J. Phys. Condens. Matter* **2009**, *187*, 012021.
[29] I. Osinnykh, T. Malin, K. Zhuravlev, *Semicond. Sci. Technol.* **2015**, *30*, 085010.
[30] M. Reshchikov, *J. Appl. Phys.* **2021**, *129*, 121101.
[31] S. McAlister, J. Bardwell, S. Haffouz, H. Tang, *J. Vac. Sci. Technol. A* **2006**, *24*, 624.
[32] K. Ranjan, S. Arulkumaran, C. Ng, A. Sandupatla, *IEEE J. Electron Devices Soc.* **2019**, *7*, 1264.
[33] Y. Qu, N. Deng, Y. Yuan, W. Hu, H. Liu, S. Wu, H. Wang, *Materials* **2022**, *15*, 3818.
[34] Y. Qin, C. Chai, F. Li, Q. Liang, H. Wu, Y. Yang, *Micromachines* **2022**, *13*, 106.
[35] L. Nasdala, D. Smith, R. Kaindl, M. Ziemann, in *Spectroscopic Methods in Mineralogy* (Eds: A. Beran, E. Libowitzky), Eotvos University Press, Budapest **2004**, pp. 281–329.
[36] Z. Feng, M. Schurman, R. Stall, *J. Vac. Sci. Technol. A* **1997**, *15*, 2428.
[37] J. Thapa, B. Liu, S. Woodruff, B. Chorpening, M. Buric, *Appl. Opt.* **2017**, *56*, 8598.
[38] H. Fujimori, M. Kakihana, K. Ioku, S. Goto, M. Yoshimura, *Appl. Phys. Lett.* **2001**, *79*, 937.
[39] B. Huang, Y. Tian, Z. Li, G. Shuguin, L. Zhaokai, *Instrum. Exp. Tech.* **2007**, *50*, 282.
[40] D. Kosemura, V. Sodan, I. De Wolf, *J. Appl. Phys.* **2017**, *121*, 035702.
[41] S. Tripathy, R. Soni, H. Asahi, K. Iwata, R. Kuroiwa, K. Asami, S. Gonda, *J. Appl. Phys.* **1999**, *85*, 8386.
[42] J. Cui, K. Amtmann, J. Ristein, L. Ley, *J. Appl. Phys.* **1998**, *83*, 7929.
[43] O. Kolomys, B. Tsykaniuk, V. Strelchuk, A. Naumov, V. Kladko, Y. Mazur, M. Ware, S. Li, A. Kuchuk, Y. Maidaniuk, M. Benamara, A. Belyaev, G. Salamo, *J. Appl. Phys.* **2017**, *122*, 155302.